E-MRS Spring meeting 2009, Symposium B

$In_x(Ga_yAl_{1-y})_{1-x}As$ quaternary alloys for quantum dot intermediate band solar cells

P. G. Linares[a]*, C. D. Farmer[b], E. Antolín[a], S. Chakrabarti[b], A. M. Sánchez[c], T. Ben[c], S. I. Molina[c], C. R. Stanley[b], A. Martí[a], A. Luque[a]

[a]*Instituto de Energía Solar, Universidad Politécnica de Madrid, Ciudad Universitaria sn, 28040 Madrid, Spain*
[b]*Department of Electronics and Electrical Engineering, University of Glasgow, Glasgow G12 8QQ, U.K*
[c]*Departamento de Ciencia de los Materiales e Ing. Metalúrgica y Q. I. Universidad de Cádiz, Campus Universitario de Puerto Real, 11510 Puerto Real, Spain*

Abstract

Within the context of quantum dot Intermediate Band Solar Cells (QD-IBSC), it is of interest to investigate the maximum value that can be achieved for the smaller of the transitions (E_L), since values larger than 0.3 eV are required for improved performance. This work provides both theoretical and experimental arguments to verify the shift of the IB position to deeper energies by using an $In_x(Ga_yAl_{1-y})_{1-x}As$ capping layer, fulfilling the double function of increasing the QD size and eliminating the discontinuity in the conduction band between the quaternary cap and the GaAs barrier.

Keywords: solar cell; Intermediate band; quantum dots; III-V quaternary materials; band alignment

1. Introduction

The IBSC concept is based on the utilization of an intermediate band (IB) material which provides a collection of energy levels in the bandgap of the semiconductor. In the case of bulk IBSC, these levels must also have their associated wave functions delocalised, in order to form a band that inhibits non-radiative recombination, and allows electronic transitions assisted by sub-bandgap photons. In this regard, the usable part of the solar spectrum and, ultimately, the solar cell efficiency are increased [1].

Since the IB has to be electrically isolated from the contacts, the voltage is assumed to be limited only by the largest of the transitions, corresponding to the host material bandgap, E_G, and not by any of the lower sub-bandgaps, E_H or E_L (see Fig. 1) [2]. The IBSC concept yields a maximum theoretical efficiency of 63.2%, surpassing the limit

* Corresponding author. Tel.: +34-91-453-3549; fax: +34-91-544-6341.
E-mail address: p.garcia-linares@ies-def.upm.es

of 40.7% [3] of single gap solar cells under maximum light concentration (the sun being assumed as a blackbody at 6000 K). The resulting optimal bandgaps are: E_G=1.95eV, E_H=1.24eV and E_L=0.71eV.

Up to now, most practical attempts to manufacture an IBSC have been based on the introduction of nanostructured stacked layers into a III-V host material. In practice, these nanostructures have to be 0-dimensional in order to provide a true zero density of states between the IB and the CB and VB, thus making the existence of three different electron gases [4] and their corresponding quasi-Fermi levels possible. Although the InAs/GaAs QD system does not satisfy the characteristics for optimal IBSC performance in terms of room temperature bandgaps (for example, E_G(GaAs)~1.42 eV), InAs/GaAs is one of the most mature QD technologies and therefore allows the fundamental principles of operation of the IBSC to be tested while reducing the uncertainties related to material processing. Furthermore, the molecular beam epitaxy (MBE) technique generally produces excellent crystalline results for this system.

It is important to compare the InAs/GaAs QD system with the ideal IBSC conception. Fig. 1 shows two different energy band diagrams under equilibrium conditions. Fig. 1a represents the ideal IBSC case for maximized efficiency, E_1>E_2>E_3, corresponding to the different photon energies available for each transition. Fig 1b illustrates a realistic InAs/GaAs QD-IBSC system with its approximate transition values. $E_{G(effective)}$ is in practice lower than GaAs bandgap due to both the levels introduced by the wetting layer (WL) next to the CB and the quasi-continuum hole confinement (due to the larger hole effective mass) within the valence band offset (VBO). The relative position of the IB (first excited electronic state) within the confinement potential is defined by the QD size and shape. It is to be noted that, in the real case, the IB is located quite close to the CB, making its associated electronic transition to the CB vulnerable to thermal escape and hence preventing the separation of both IB and CB populations.

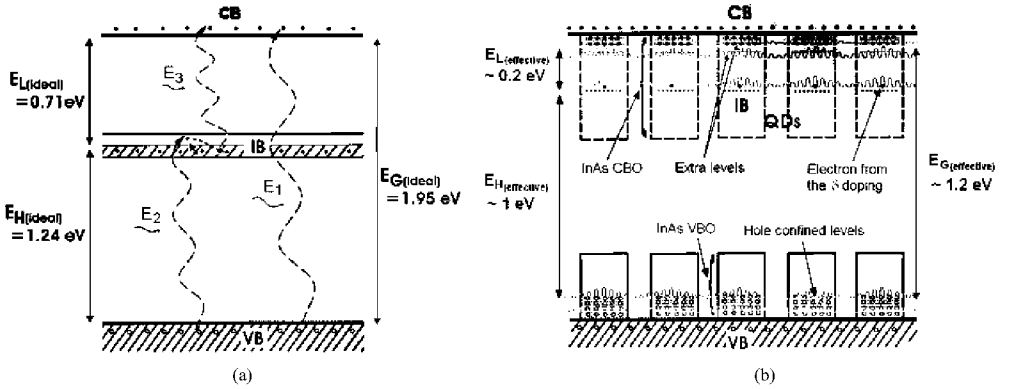

Fig. 1. IBSC band diagram: a) Ideal case; b) InAs/GaAs QD system with approximate values for CBO, VBO and band transition energies. Approximate confined electron wavefunctions and δ-doping responsible for the partial filling of the QD levels are also shown.

From the previous discussion, the necessity for deeper QD electron levels within the conduction band offset (CBO) is apparent and this could be achieved, in principle, with larger QDs. However, as will be shown in the following sections, lowering the IB position is a trade-off between maintaining a sufficiently high areal density of QDs, whilst at the same time obviating the impact on recombination of the undesirable appearance of extra levels between the IB and CB.

2. Method description

The InAs/GaAs QD samples in this paper were grown in the Stranski-Krastanov (S-K) mode [5] which leads to an almost inverse dependence between dot size and density (the larger the dot size, the lower the QD density) that

can be controlled to some extent through the MBE growth parameters (arsenic over-pressure, substrate temperature, growth rate, etc.). Since QD-IBSCs require the highest possible volumetric density of QDs (to maximize absorption through the IB), a large size must be accompanied by both high areal density and a large number of individual layers of QDs. In this regard, strain-induced alloying during QD capping with GaAs which acts to reduce the QD size has been circumvented by depositing a capping layer containing In, immediately above each layer of QDs [6]. The In incorporation occurs by means of a surface process in which In and other Group III adatoms are exchanged during the deposition of the capping layer above the QD InAs layers. The driving force for such redistribution is the strain field appearing during QD formation, responsible for the preferable relocation of indium adatoms next to InAs islands (Fig. 2)This is then followed by a GaAs spacer layer into which Si δ-doping is introduced to provide the electrons for half-filling the IB by modulation doping. The layer sequence is repeated to form a QD stack.

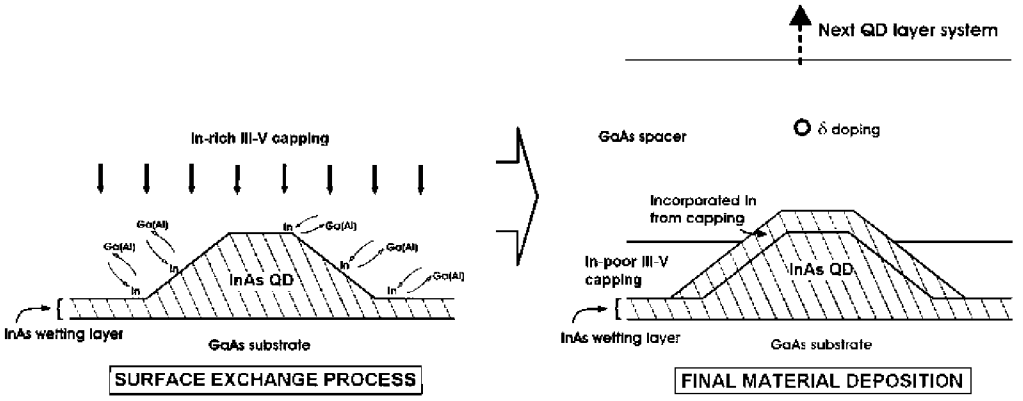

Fig. 2. Sketch showing the In incorporation process. On the left side, the surface exchange process is shown. The right side represents the steady state case where most of the In in the capping layer has joined the InAs island contributing to QD enlargement [6].

There is a limit to the total amount of In that can be deposited directly during QD formation and the subsequent capping of the dots with a strain-relieving buffer before strain relaxation occurs, an effect reported by Ustinov et al. [6]. The total amount of InAs Q_Σ measured in monolayers (ML) deposited in the QDs and the cap can be expressed by the following the relationship:

$$Q_\Sigma = Q_{InAs} + x\, L_Z, \qquad (1)$$

where Q_{InAs} is the initial amount of InAs deposited for QD nucleation (usually ~2.5ML), x is the In compositional fraction of the capping layer and L_Z its thickness.

Several issues have still to be considered. First, the accumulated amount of InAs in the QDs and cap cannot exceed 5ML [6], otherwise the QDs relax and their associated photoluminescent emission (PL) intensity decreases as non-radiative recombination of excess carriers at dislocations takes place. Second, the maximum In stoichiometry of the cap is found to be approximately 0.2 without QD performance degradation. This empirical value has been corroborated through low temperature photoluminescence (PL) measurements on structures with different $In_xGa_{1-x}As$ cap compositions as shown in Fig. 3. In this plot, the dotted curve corresponding to x=0.21 shows the largest redshift (deepest QD energy level) while still retaining a strong PL intensity. Finally, the third condition refers to a zero CBO to prevent the appearance of either a detrimental intermediate energy band between the IB and CB (positive CBO) and consequent voltage loss, or a potential barrier (negative CBO) that obstructs the electron transport through out the CB (although this barrier might help to increase the photon absorption from the IB to the CB) [7].

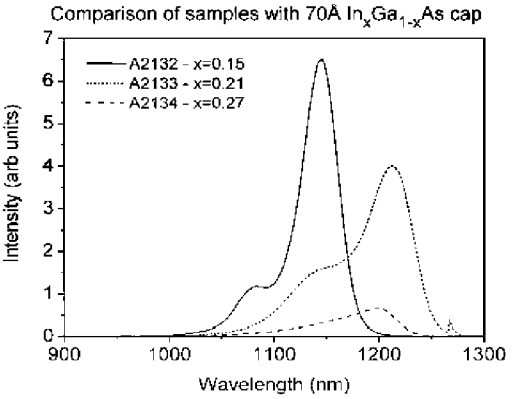

Fig. 3. Low temperature (T=10K) PL measurement showing In incorporation on $In_xGa_{1-x}As$. Sample with x=0.15 has presumably not incorporated enough In and therefore peaks at approx. 1150nm; conversely, sample with x=0.27 probably has an excess of In incorporation leading to excessive dislocations and a significant reduction in its integrated PL intensity; sample with x=0.21 shows both a red shifted (over 1200nm) and intense PL spectrum.

To fulfil of all these constraints, a III-V quaternary alloy is used. The choice of $In_x(Ga_yAl_{1-y})_{1-x}As$ as an appropriate capping material as well as a theoretical model that allows the calculation of its correct stoichiometry are explained in next section.

Another technique used for QD size enlargement is worth mentioning. It is based on the control of the InAs material quantity and spacer thickness of the first QD layer (named seed layer) so that residual vertical strain originating from this first layer acts as the driving force for the nucleation of the next QD layers. The critical thickness for the appearance of QDs in the second QD layer is reduced, and a higher fraction of the deposited InAs feeds into the QDs, making them bigger. The seed layer is characterized by a slightly larger amount of InAs deposition (2.7ML instead of 2.5ML). A consequence is vertical alignment of QDs, whilst the QD density in the following layers remains roughly as high as in the seed layer, but with an increased dot size and a thinner WL.

3. Optimization of the $In_x(Ga_yAl_{1-y})_{1-x}As$ quaternary capping

The MBE growth process is simplified by using a single Group V element, arsenic, throughout the structure. Flexibility in the design of the properties of the capping layer flows from the use of the quaternary $In_x(Ga_yAl_{1-y})_{1-x}As$ whose band gap and CBO with respect to GaAs can be tailored via the compositional fraction of In (x) and the proportion of Al:Ga. A heterojunction energy band alignment model that includes hydrostatic strain effects has been developed for this purpose. The theoretical model used for the calculation of the band alignment between the $In_x(Ga_yAl_{1-y})_{1-x}As$ quaternary capping material and the GaAs barrier material is mainly based on the Model Solid Theory (MST) by Van de Walle [8].

The calculation of the quaternary heterojunction band offsets is carried out through interpolation from known binary III-V electronic parameters, which sometimes also requires knowledge of their respective ternary and quaternary bowing parameters (BP) [9]. The required parameters are listed in Table 1, where the necessary data input and interpolation method are also described.

Depending on the parameter to be calculated for the quaternary alloy, the method to estimate it can consist of either a linear interpolation from its constituent binary data (B_i with i=1,2,3) as indicated in Eq. 2 or a non-linear

interpolation through their ternary and quaternary BP (C_{ij} and D, respectively) of Eq. 3 [9, 10]. If the parameter to be calculated is an electronic level, its ternary BP (*T in this case*) should then be estimated by means of Eq. 4 [8].

$$Q\{(B_2)_x[(B_1)_y(B_3)_{(1-y)}]_{1-x}\}=y(1-x)B_1+xB_2+(1-x)(1-y)B_3 \quad (2)$$

$$Q\{(B_2)_x[(B_1)_y(B_3)_{(1-y)}]_{1-x}\}=y(1-x)B_1+xB_2+(1-x)(1-y)B_3+x(1-x)(1-y)C_{23}+ x(1-x)yC_{12}+ (1-x)y(1-y)C_{13}+x(1-x)y(1-y)D \quad (3)$$

$$T[B_xC_{(1-x)}A]=3[-a_i(AC)+a_i(BC)]\Delta a/a_o \quad (4)$$

In these equations, Q is the quaternary parameter to be calculated; x and y are the different stoichiometric proportions; a_i are the VB or CB deformation potentials; a_0 is the bulk material lattice constant; Δa is the difference in lattice constant; and $\Delta a=a_i(AC)-a_i(BC)$. The suitability of each equation depends on the parameter being determined and the availability of data in each case, as show in the third column of Table 1.

Table 1. Different parameters required for the Van de Walle algorithm band alignment calculation: bandgap (E_G), lattice constant (a_l), hydrostatic deformation potentials for VB and CB (a_v and a_c respectively), average of the three uppermost VB ($E_{v,av}$), spin-orbit splitting (Δ_0) and elastic constants (C_{11}, C_{22}, C_{44}), together with their necessary data input and with the proper equation to be used in each case for their interpolation.

Parameter	Data input	Interpolation method
E_G	B_1, B_2, B_3, C_{12}, C_{13}, C_{23}, D	Eq. 3
a_l	B_1, B_2, B_3	Eq. 2
a_v	B_1, B_2, B_3	Eq. 2
a_c	B_1, B_2, B_3	Eq. 2
$E_{v,av}$*	B_1, B_2, B_3, a_{l1}, a_{l2}, a_{l3}	Eq. 4 (for the ternary BP) and Eq. 3
Δ_0*	B_1, B_2, B_3, C_{12}, C_{13}, C_{23}	Eq. 3
C_{ii} $(i=1,2,4)$	B_1, B_2, B_3	Eq. 2

*There are no data for the quaternary BP

The MST takes into account the hydrostatic stress derived from changes in the unit cell caused by the lattice mismatch. This model predicts a modification of the band alignment that is proportional to the parallel and perpendicular strain tensors and deformation potentials at both the CB and VB. The hydrostatic stress appearing on the material interface also depends on both material thicknesses and crystal orientations. The result of the calculations fulfilling the three conditions is plotted in Fig. 4. The vertical dashed line shows the optimal Al content and, therefore, the global stoichiometry that the quaternary barrier material must have. Its final composition is $In_{0.2}Al_{0.23}Ga_{0.57}As$.

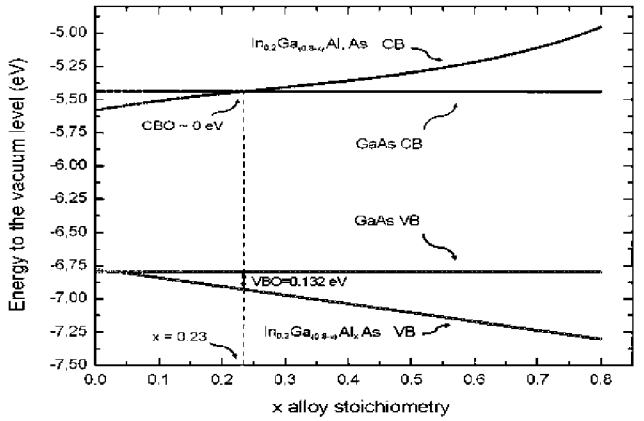

Fig. 4. Calculated band diagram showing GaAs and $In_{0.2}Ga_{(0.8-x)}Al_xAs$ VB and CB lineups depending on the x stoichiometric value (Al fraction in this case). Optimal x is chosen so the CBO is zero.

4. Experimental results

Several test devices have been manufactured to demonstrate the validity of the theoretical arguments. A sketch of the cell structure for sample A2219 is shown in Fig. 5. It represents a 10-layer InAs/GaAs QD solar cell and includes an InAlGaAs quaternary capping layer. A seed layer is included as part of the QD size enlargement technique. The aforementioned Si δ-doping is also included in each of the GaAs spacers and is responsible for the partial filling of the IB [11]. The structure is completed with an AlGaAs BSF, a window layer and the so-called field damping layers, to prevent tunnelling from the IB to the CB and to locate the IB within a flat band region [12].

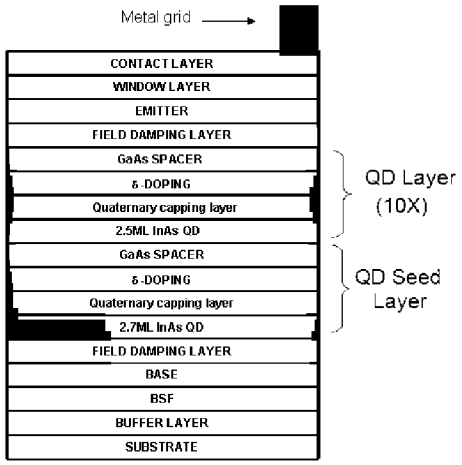

Fig. 5. Sketch of the different layers of the A2219 QD solar cell.

Fig. 6 shows the results of absolute external quantum efficiency (QE) measurements. A2219 sample (solid line) is compared to a previous QD solar cell (hollow circles) without quaternary capping layers, and also to a GaAs reference (hollow triangles) solar cell. From the QE measurements, it is clear that QD solar cells show increased IR absorption beyond the limit of GaAs (approx. 870nm) through the VB-IB transition. Then, if both QD-IBSC are compared, a further extension into the infrared of the QE is observed for A2219. The latest suggests that the size enlargement technique proposed in this paper is suitable for an IB redshift of at least 100nm beyond that achieved without the quaternary capping layer.

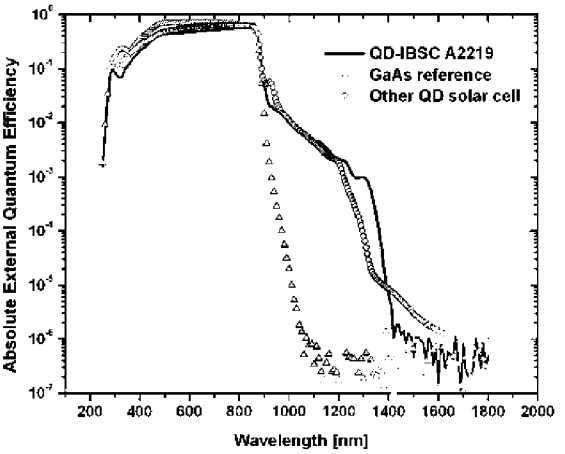

Fig. 6. Absolute external QE of sample A2219 (solid line) compared to a QD solar cell without quaternary capping layer (hollow circles) as well as to a GaAs reference solar cell (hollow triangles). A clear redshift mainly attributed to the QD size enlargement can be observed.

As it has been mentioned earlier, lowering the IB is a necessary condition for achieving an increased separation between the IB and CB electronic populations, which is also needed for good IBSC performance. Unfortunately, although lowering of the IB within the bandgap has been achieved, the QD-IBSC global performance has not been improved. This is due to degradation of the emitter caused by the accumulation of strain throughout the ten QD layers, as previously reported in reference [13]. It is shown by the TEM image of Fig. 7, where threading dislocations are observed above the QD layers. A feasible solution to this last problem has been implemented through the introduction of strain-compensation layers, widely discussed in references [14] and [15].

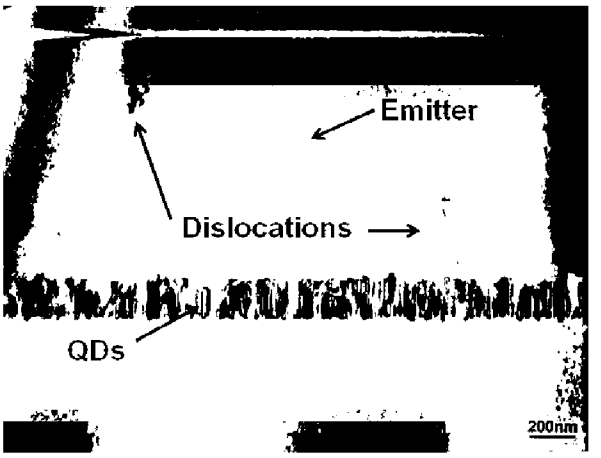

Fig. 7. TEM image of sample A2219. Dislocations are present in the vicinity of the last QD layer and in the emitter. This effect is mainly caused by vertical strain accumulation throughout the ten QD layers.

Some extra levels appearing over the IB are expected, especially if larger QDs are fabricated. However, their harmful effects (extra recombination and thermal escape), responsible for an open circuit voltage V_{OC} limited by the E_H transition, are expected to be minimized through their use under high concentrated light [12]. Nevertheless, the actual difficulties in their manufacture, such as the emitter degradation, still have to be overcome.

5. Conclusions

Optimizing the performance of the QD-IBSC requires an enlargement of the bandgap E_L that separates the IB from the CB. This implies lowering the energy associated with the IB which can be obtained through enlargement of the QD size. In this work, we have investigated and shown the feasibility of using a quaternary cap to achieve a significant redshift. However, the quantum efficiency measurements also reveal degradation in the performance of the emitter of the cell, confirmed through TEM analysis.

Acknowledgement

This work has been supported financially by the European Commission through the project IBPOWER (Ref. No. Grant Agreement No. 211640), by the GENESIS FV project of the National Spanish program CONSOLIDER (Grant No. CSD2006-0004), and by La Comunidad de Madrid through the funding of the project NUMANCIA (Ref. No. S-0505/ENE/0310).

References

[1] A. Luque, A. Martí, E. Antolín, and C.Tablero, "Intermediate bands versus levels in non-radiative recombination", *Physica B*, Vol. 382, p. 320-327, 2006.

[2] A. Luque and A. Martí, "Increasing the efficiency of ideal solar cells by photon induced transitions at intermediate levels", *Phys. Rev. Lett.*, Vol. 78, p. 5014–5017, 1997.

[3] W. Shockley and H. J. Queisser, "Detailed Balance Limit of Efficiency of p-n Junction Solar Cells", *J. Appl. Phys.*, Vol. 32, p. 510-519, 1961.
[4] A. Martí, L. Cuadra and A. Luque, "Quantum dot intermediate band solar cell" *Conference Record of the 28th IEEE Photovoltaics Specialists Conference*, p. 940-943, 2000.
[5] M. Sugawara, "*Self-assembled InGaAs/GaAs quantum dots*", Vol. 60: Academic Press, New York, 1999.
[6] V. M. Ustinov et al., "Long-wavelength emission from self-organized InAs quantum dots on GaAs substrates", *Microelectronics Journal*, Vol. 31, p. 1-7, 2000.
[7] A. Martí et al., "Progress in quantum-dot intermediate band solar cell research," *in Proc. of the 21st European Photovoltaic Solar Energy Conference*, J. Poortmans, H. Ossenbrink, E. Dunlop, and P. Helm, Eds. Munich: WIP-Renewable Energies, 2006, pp. 99-102.
[8] C. G. Van de Walle, "Band lineups and deformation potentials in the solid model theory", *Phys. Rev. B*, Vol. 39, No. 3, p. 1871-83, 1989.
[9] I. Vurgaftman et al., "Band Parameters for III-V compound semiconductor and their alloys", *J. Appl. Phys.*, Vol. 89, No. 11, p. 5815-75, 2001.
[10] G. P. Donaty et al., "Interpolating semiconductor alloy parameters: Application to quaternary III-V band gaps", *J. Appl. Phys.*, Vol. 94, No. 9, p. 5814-19, 2003.
[11] A. Martí, L. Cuadra and A. Luque, "Design constraints ofthe quantum-dot intermediate band solar cell", *Physica E*, Vol. 14, p. 150-157, 2002.
[12] A. Martí et al., "Elements of the design and analysis of quantum-dot intermediate band solar cells", *Thin Solid Films*, Vol. 516, p. 6716–6722, 2008.
[13] A. Martí et al., "Emitter degradation in quantum dot intermediate band solar cells", *Appl. Phys. Lett.*, Vol. 90, p. 233510, 2007.
[14] R. Oshima, A. Takata and Y. Okada, "Strain-compensated InAs/GaNAs quantum dots for use in high-efficiency solar cells", *Appl. Phys. Lett.*, Vol. 93, p. 083111, 2008.
[15] V. Popescu et al., "Theoretical and experimental examination of the intermediate-band concept for strain-balanced (In,Ga)As/Ga(As,P) quantum dot solar cells", *Phys. Rev. B*, Vol. 78, p. 205321, 2008.